ORNL/SPR-2019/1240

Comparative Analysis of Nondestructive Examination Techniques of Enhanced Model Based Iterative Reconstruction (MBIR) and Frequency-banded Synthetic Aperture Focusing Technique (SAFT) Reconstructions

N. Dianne Bull Ezell
S. V. Venkatakrishnan
Hector Santos-Villalobos
Austin Albright

September 2019

OAK RIDGE NATIONAL LABORATORY
MANAGED BY UT-BATTELLE FOR THE US DEPARTMENT OF ENERGY

ORNL/SPR-2019/1240

Reactor and Nuclear Systems Division

COMPARATIVE ANALYSIS OF NONDESTRUCTIVE EXAMINATION TECHNIQUES OF ENHANCED MODEL-BASED ITERATIVE RECONSTRUCTION (MBIR) AND FREQUENCY-BANDED SYNTHETIC APERTURE FOCUSING TECHNIQUE (SAFT) RECONSTRUCTIONS

N. Dianne Bull Ezell
S.V. Venkatakrishnan
Hector Santos-Villalobos
Austin Albright

Date Published: September 2019

Prepared by
OAK RIDGE NATIONAL LABORATORY
Oak Ridge, TN 37831-6283
managed by
UT-BATTELLE, LLC
for the
US DEPARTMENT OF ENERGY
under contract DE-AC05-00OR22725

CONTENTS

LIST OF FIGURES

ACRONYMS

AI	artificial intelligence
ASR	alkali silica reaction
CNN	convolutional neural network
DDL	direct deep learning
DOE-NE	US Department of Energy Office of Nuclear Energy
DPC	dry point of contact
EPRI	Electric Power Research Institute
FB-SAFT	frequency-banded synthetic aperture focusing technique
FN	false negative
FOV	field-of-view
FP	false positive
L-MBIR	linear-MBIR
MAP	maximum a posteriori probability
MBIR	model-based iterative reconstruction
MRF	Markov-random field
NDE	nondestructive evaluation
ORNL	Oak Ridge National Laboratory
PR	precision vs. recall
SAFT	synthetic aperture focusing technique
SGD	stochastic gradient descent
TP	true positive
U-MBIR	ultrasonic MBIR

ACKNOWLEDGMENTS

This work is funded by the US Department of Energy Office of Nuclear Energy under the Light Water Reactor Sustainability program through the Materials Research Pathway. The authors would like to thank Dr. Lev Khazanovich at the University of Pittsburgh for acquiring the data used to develop the reconstruction techniques.

EXECUTIVE SUMMARY

As the existing US fleet of nuclear power plants (NPPs) approach their expected lifetimes and only a few new reactors are coming online, the industry is looking to extend their licenses beyond 60 years and improve efficiencies through research-informed aging management programs. Reinforced concrete is an inexpensive, strong material widely used in the nuclear industry. However, it is not invulnerable to fatigue and damage. Degradation mechanisms in reinforced concrete include delamination, air gaps, foreign materials or items lost in the concrete during pouring, corrosion, irradiation-induced cracking and alkali silica reaction (ASR). Shortly after the discovery of ASR in the Seabrook nuclear power plant in 2010 [1], the Light Water Reactor Sustainability program under the US Department of Energy (DOE) Office of Nuclear Energy (NE) has funded Oak Ridge National Laboratory (ORNL) to study the effects of ASR in concrete.

While nondestructive evaluation (NDE) of infrastructure materials is a well-known, well-understood technology, the relationship between the measurement process and the material is less developed than the instrumentation. In collaboration with Purdue University, ORNL has been developing image reconstruction algorithms that are more powerful than techniques currently used by industry. Specifically, ORNL investigated the reconstruction of ultrasonic tomography data acquired from concrete specimens using the MIRA system, developed by Germann Instruments [2]. Ultrasonic tomography is an effective measurement modality for detecting ASR in part due to the ability of ultrasonic frequencies to travel well below the surface of concrete structures depending on the frequencies and power of the ultrasonic wave. The ultrasonic tomographic images reconstructed from MIRA measurements are typically generated using the synthetic aperture focusing technique (SAFT). However, these images can be distorted with noise and stitching errors. Through this research, ORNL has developed several improved image reconstruction techniques. First, ORNL applied wavelet packet decomposition that ultimately yielded frequency-banded SAFT (FB-SAFT). While FB-SAFT provided improvements in interpretability and the clarity of reconstructed image, the research team recognized that further advancement was needed, which led to Ultrasonic Model-Based Iterative Reconstructions (U-MBIR). Shortly thereafter, U-MBIR led to the development of direct deep learning (DDL) reconstructions.

This report reviews progress on the development of these reconstruction techniques and compares how well they reconstruct the same images with the upgraded algorithms. Specifically, the improvement between MBIR and DLL reconstructions, how SAFT can be used to improve reconstruction time for MBIR and DDL, and further development considerations for FB-SAFT are reviewed herein. FB-SAFT improves the artifacts and noise in the background on images, MBIR and DDL improve noise and stitching effects, but all three methods are a large improvement on standard SAFT reconstructions.

1. INTRODUCTION

Industry continues to work to create better ultrasonic instruments for NDE of concrete infrastructures. Organizations like the Electric Power Research Institute (EPRI) are developing guidance and training programs whose goals are to ensure that users are accurately and reliably performing NDE measurements. It is within this context that ORNL has focused on the improvement of the reconstruction algorithms that can be applied to data collected using commercially available systems and ultimately to be utilized by the people trained to use and assess the structural integrity of nuclear power plant's concrete infrastructure.

Several technologies were investigated for NDE of thick concrete structure, including ultrasonic linear array, ground-penetrating radar, air-coupled impact-echo, air-coupled ultrasonic surface wave, and semi-coupled ultrasonic tomography [3]. Each of these techniques has pros and cons, but it was demonstrated that ultrasonic inspection is the best option for concrete NDE due to its ability to penetrate thick concrete structures. Using a single ultrasonic instrument, high frequencies can detect edges and small defects, but only close to the surface. However, low frequencies can penetrate deeper into the concrete, but the size of defects and structures that will they will miss, with respect to the frequency's wavelength, small defects and structures.

In FY19, the image processing development team continued to improve the reconstruction techniques beyond that previously reported [4]. These improvements include the development of direct deep learning (DDL) image reconstruction technique.

2. ULTRASONIC TOMOGRAPHY AND SAFT RECONSTRUCTION

The ultrasonic data collected and used with these reconstruction techniques were collected using a MIRA unit, which is a commercially available ultrasonic inspection device. The MIRA system is based on an ultrasonic pulse-echo method. The instrument uses an array of 40 dry-point contact (DPCs) transducers that transmit and receive the ultrasonic signals [5]. The transducers form a 10-channel (4 × 10 array) instrument by first "firing" the four transmitters in the first column to form the impulse signal, and then receiving on the other 9 columns, as illustrated in Figure 1.

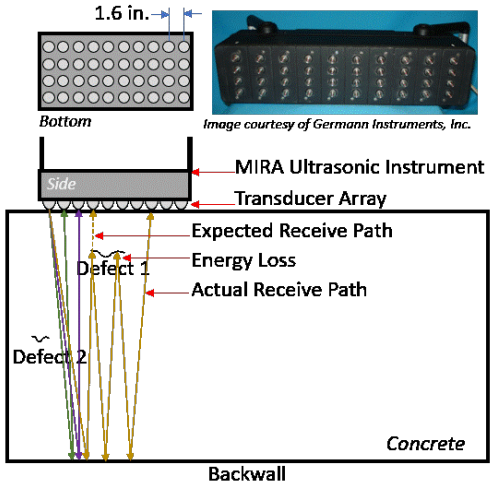

Figure 1. Ultrasonic NDE (images courtesy of Germann Instruments, Inc.).

MIRA has an adjustable frequency range of 28–85 kHz. The DPC transducers of the MIRA were designed to produce a shear wave with a nominal frequency of 50kHz [2] and all the data in this report was collected with the frequency set to 50 kHz. The received signals collected by the MIRA and stored by the system treat each column of four DPCs as a single entity. The individual signals of each DPC being used as a receiver are not user accessible. Thus, the system produces 45 unique impulse time-history measurements by automatically cycling through the unique combinations of the transmitting column and the receiving columns [5]. The 45 unique measurement sequences collected result in the following sets of fixed horizontal spacing between the transmitting and receiving columns of the DPCs' nine unique pairings with 40 mm (1.6 in.) spacing, eight unique pairings with 80 mm (3.1 in.) spacing, seven unique parings with 120 mm (4.7 in.) spacing, six unique pairings with 160 mm (6.3 in.) spacing, etc., down to one unique pairing with 360 mm (14.2 in.) spacing [6]. Each of these 45 unique transmitter and receiver pairings generate an A-scan, as shown in Figure 2 and Figure 3. Each time the MIRA is activated a set of these 45-unique A-scans is acquired.

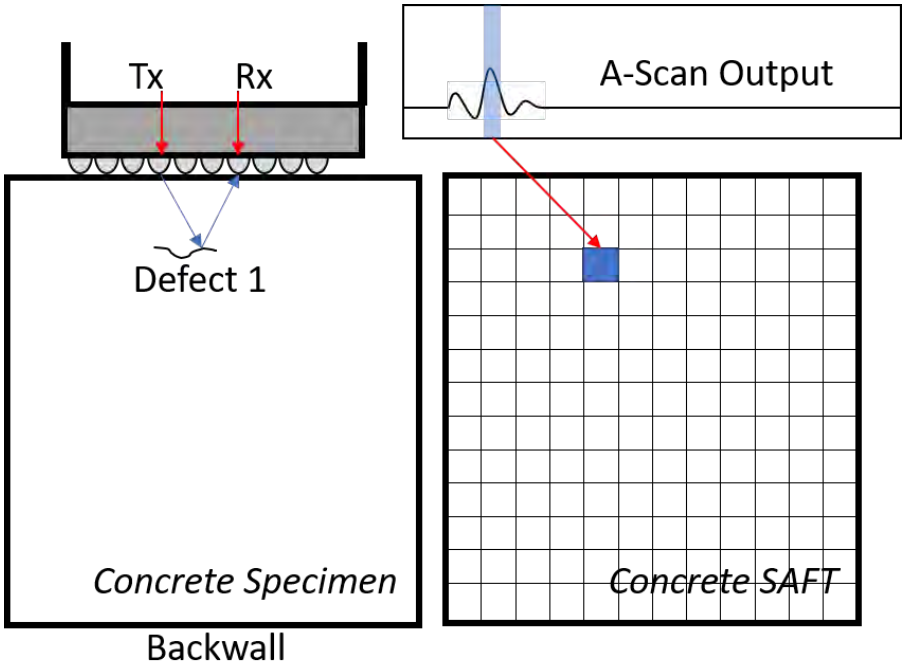

Figure 2. Illustration of MIRA instrument generating SAFT reconstruction.

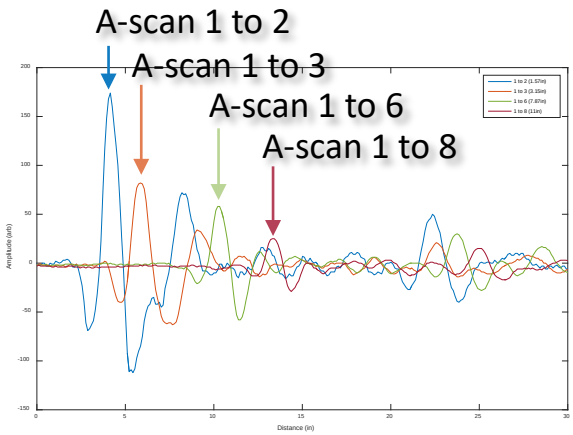

Figure 3. Illustration of A-scan data with column 1 of transducers transmitting to receiving columns 2, 3, 6, and 8.

Using the fixed, known spacings between the transmitting and receiving columns of the MIRA array, the propagation velocity estimated from the direct arrival wave propagating along the test specimen's face, and the collected A-scan signals provide all the necessary inputs and parameters for applying the synthetic aperture focusing technique (SAFT).

SAFT is a delay-and-sum technique commonly used to reconstruct time-of-flight ultrasonic signals. The round-trip distance is calculated for each depth for a transmitter and receiver pair by converting the time to distance using the propagation velocity of the material. While SAFT is a well-developed tomographic technique that is used widely throughout the nondestructive evaluation and testing industry, it does suffer from artifacts and background noises in the reconstructed B-scan images that make it difficult to identify internal structure and content – especially in porous, grainy materials like structural concrete. For this reason, ORNL developed a frequency-banded SAFT (FB-SAFT) [7].

Typically, a grid is drawn on the surface of the concrete to define the boundary of the measurement and the scanning path [8], as shown in Figure 4. This also helps when repeatedly placing the instrument for each measurement. The yellow line shown in Figure 4 represents the scanning path along line 3 of the grid. The instrument is placed with the first marking (on the MIRA's casing) aligned at the grid location (3, A), and then it is stepped along line 3, aligning the same MIRA casing mark with at each of the intersections of a lettered grid line with the scan line, line 3 in this example. This acquires data at (3, A), (3, B),…, (3, H), and (3, I). Redundant data are intentionally acquired as the instrument is moved along the scan line (Figure 5). This process is repeated at each number line 1-9 collecting an acquisition at the intersection of each letter grid. Then the MIRA instrument is rotated 90 degrees and is scanned along the lettered lines (A-I), collecting an acquisition at the intersection of each numerically identified gridline.

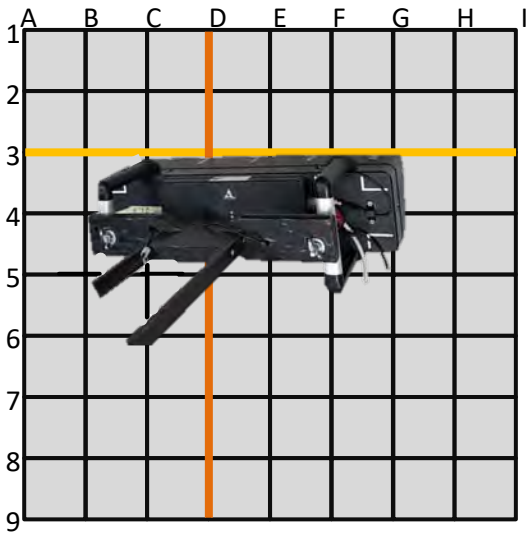

Figure 4. Measurement boundary and scanning path (yellow line defines 3-scan; orange defines D-scan).

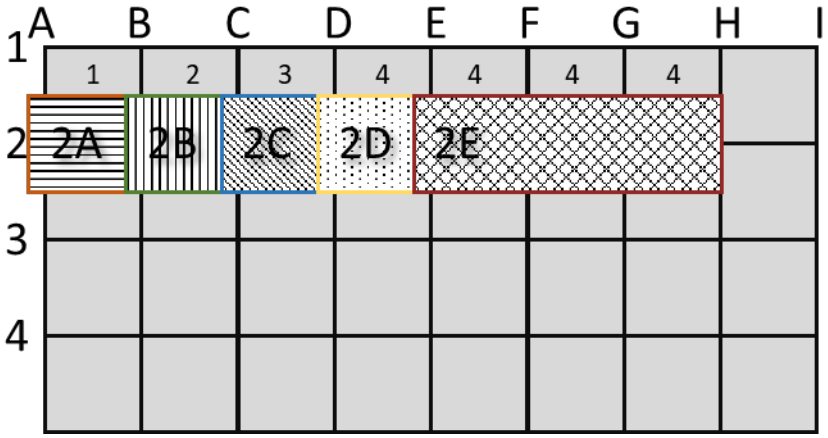

Figure 5. MIRA scanning measurement along a line. Note the overlapping areas where "redundant" data is acquired, the small numbers of above the different boxes labeled 2A, 2B, 2C, etc. identifies how many times an acquisition was made that covered that grid cell.

3. DEVELOPMENT OF FREQUENCY-BANDED SAFT USING WAVELETS

Frequency-banded SAFT (FB-SAFT) modifies the typical SAFT workflow by dividing the time-series data into frequency bands using a wavelet technique and then performing the SAFT reconstruction on the decomposed bands (Figure 6) [9]. This technique is based on wavelet packet decomposition. The sample rate of the MIRA system is 1 MHz resulting in a bandwidth of 500 kHz due to the Nyquist criteria. The original time series data contains all 500 kHz of the bandwidth and is called node 0. Applying wavelet packet decomposition to the node 0 data decomposed the data into two portions known as: the *approximate*, and the *detail*. The approximate portion contains low-pass coefficients from the wavelet decomposition and using wavelet packet numeric naming convention would be called node 1. Likewise, the detail portion contains the high-pass coefficients and called node 2 in the numeric naming convention. Therefore, nodes 1 and 2 are the decompositions of node 0. Node 1 contains the lower half of the

bandwidth (0–250 kHz), and node 2 contains the upper half of the bandwidth (250–500 kHz). Nodes 1 and 2 are each decomposed in the same manner as node 0, generating an approximate and detail portion from node 1 and 2. Node 3 and node 4 being the approximate and detail respectively from node 1 and the likewise for node 2 but named node 5 and 6. This process continues through several iterations (Figure 6). A user can view each FB-SAFT reconstruction of each node at their discretion. Since the center frequency of the MIRA system used during the data acquisition was 50kHz nodes, a.k.a. frequency bands that contained this frequency were examined. Using the FB-SAFT method [7] and the wavelet node containing the nominal center frequency of the MIRA has repeatedly shown a reduction in background scatter noise and results in crisply resolved images of internal structures and defects [9]. Reconstructions using node 16, which contains the energy content found in the frequencies from 31.25 kHz to 62.5 kHz, display significantly reduced background scatter noise, improved resolution, and fewer artifacts.

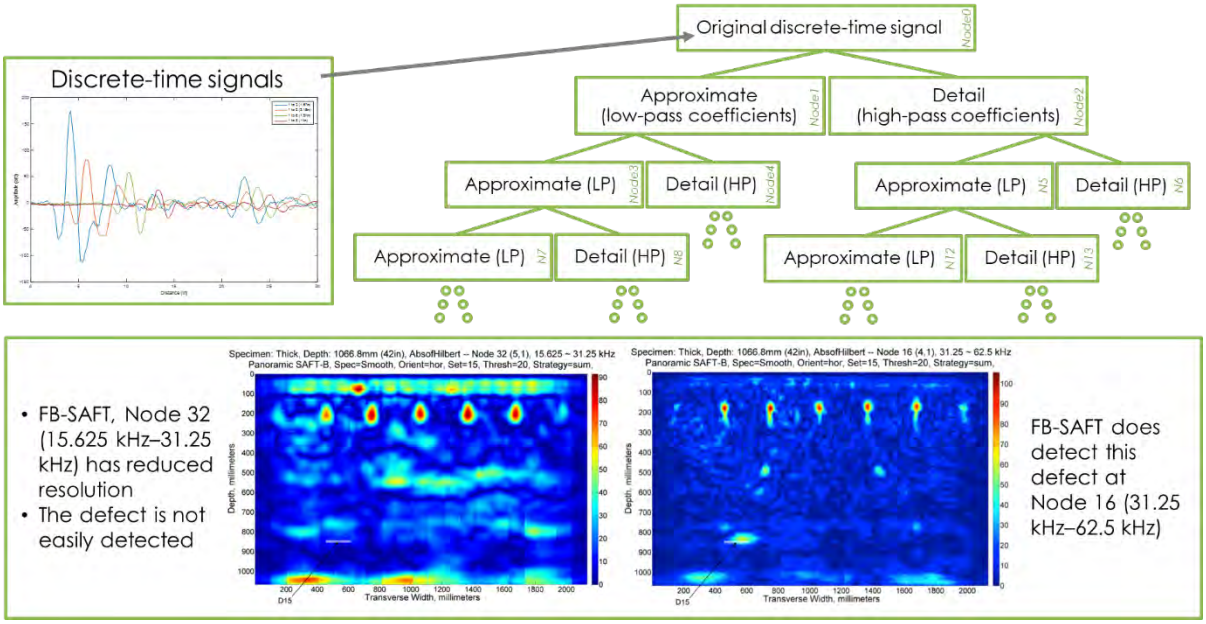

Figure 6. Illustration of FB-SAFT reconstruction technique.

This reconstruction technique was developed using ultrasonic data measured from a 10-inch thick specimen. In the color-based map generated using the signal amplitudes, deep blue represents low energy reflections, and red represents high energy reflections. The reconstructions displayed in Figure 6 are from node 32 (15.625–31.25 kHz) and node 16 (31.25–62.5 kHz). In node 16, the background scatter noise in the middle of the images is greatly reduced, the rebars reconstruct with more vivid and sharper edges, the defect is easier to detect (noted on the image), and the surface reflections are greatly reduced. The poor quality of the node 32 reconstruction is indicative of too narrow a frequency band and thus the reduced energy content of the band is inadequate for producing a clear, sharp reconstruction. This same fact, lack of energy, is directly applicable to applying FB-SAFT or any pulse-echo technique to thick concrete specimens. If a majority of the ultrasonic energy that propagates into the specimen is absorbed before reflecting back to the receivers there is little that can be done to improve the reconstruction as without reflected energy to receive there is little to no information to extract. One approach is to stitch together multiple B-scan images to create a B-scan with a much wider field of view as seen in Figure 7, which displays a panoramic SAFT reconstruction [10]. As part of this stitching, any redundant data collected by overlapping the acquisitions as the instrument is moved, Figure 5, and is integrated providing a straight forward way to increase the energy/information acquired in addition to providing the panoramic SAFT reconstruction with the ability to yield a B-scan of the entire scan line.

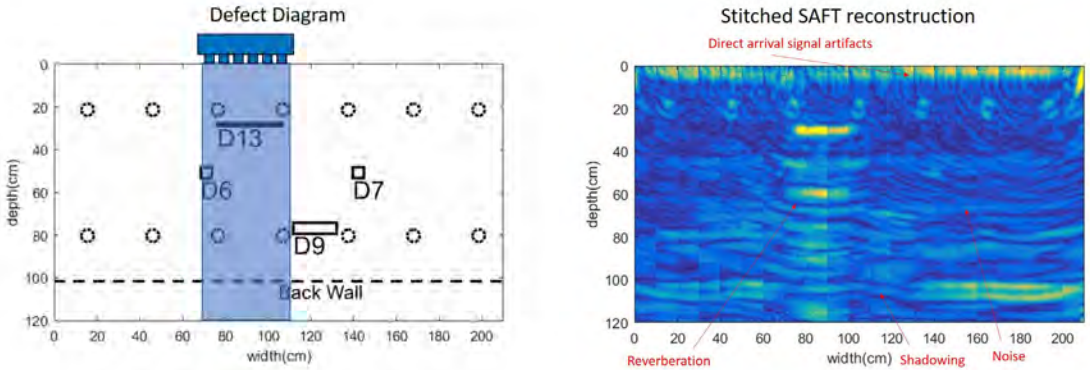

Defect diagram containing steel rebars (dotted circles), defects (marked D#), and the back wall (dotted line)

SAFT reconstruction for the entire field-of-view after stitching the results from each individual scan

Figure 7. Example of a SAFT reconstruction from real data of a concrete structure.

When applying SAFT and FB-SAFT to fabricated concrete specimens, 6-feet and 7-feet thick, it was found that reconstructed images that appear to lack a backwall reflection should be treated cautiously with respect to the deeper depths of the reconstructed image. As the lack of a backwall reflection is indicative of a significant amount of the ultrasonic energy being absorbed and/or dissipated without reflecting back to the receiving transducers. In consideration of the need to extract more "information" in such challenging environments additional reconstruction methods have been developed in parallel.

4. DEVELOPMENT OF ULTRASONIC MODEL BASED ITERATIVE RECONSTRUCTION

To address these challenges, ORNL developed model-based iterative reconstruction (MBIR) techniques for the ultrasound inversion [11] of data scanned from a large field of view. These techniques involve formulating the reconstruction as a maximum a posteriori probability (MAP) estimation problem of the form:

$$x_{MAP} = \arg\min_{x} \{-\log p(y|x) - \log p(x)\},$$

where x is the ultrasound image to be reconstructed, y is the measured data, x_{MAP} is the reconstructed image, p(y|x) is the forward model and the probability distribution of y given x, and p(x) is the prior model and the probability distribution of x. This formulation is equivalent to minimizing a cost function, where the first term is a *data-fidelity* term, and the second is a *regularization* term. ORNL developed a *linear forward model* that accounts for the direct arrival of the ultrasound signal, the delay in the received signal due to various reflections, attenuation effects in the sample, and the presence of Gaussian measurement noise. This model also accounts for the shape of the ultrasound beam generated by the transducer. The algorithm combines the model with a *Markov-random field (MRF) prior model* to account for correlations between adjacent regions in a typical image, as well as the loss of resolution in the deeper regions of the sample being investigated. Furthermore, unlike existing techniques that process individual scans separately and then stitch the results together, the ORNL model jointly accounts for all the measurements made in the entire scan. Formally, the MBIR ultrasound reconstruction is formulated as follows,

$$(x, g, \sigma^2)_{MAP} = \arg\min_{x\geq 0, g, \sigma^2} \left\{ \frac{1}{2\sigma^2} \|y - Ax - Dg\|^2 + \frac{MK}{2} \log(\sigma^2) + \sum_{\{s,r\}\in C} b_{s,r}\ \rho(x_s - x_r, \sigma_{g_{s,r}}) + \sum_{s\in S} \frac{x_s}{\sigma_{e_s}} \right\},$$

where A represents the linear propagation matrix, D is a matrix representing the direct arrival signal, g is a scaling for the direct arrival signal, σ is the standard deviation of the measurement noise, $b_{s,r}$ is a set of weights between neighboring voxels, $\rho(.)$ is a MRF-based penalty applied to the difference between neighboring voxels, and σ_g and σ_e are smoothing parameters [9], [12]. A fast algorithm was also developed based on an iterative coordinate descent technique to minimize the above cost function rapidly to obtain near real-time results.

To quantitatively evaluate the ability of different algorithms to detect known defects, a method based on pixel-wise precision-recall curves was introduced. A pixel-wise precision-recall test calculates the number of true positives (TPs), false positives (FPs), and false negatives (FNs) for each technique. These values are used to plot the precision vs. recall (PR) curves, where,

$$recall = \frac{TP}{TP+FN}, \text{ and}$$

$$precision = \frac{TP}{TP+FP}.$$

This detection test compares the performance of each technique by the area under the PR curve. The larger the area, the better the technique. To use this for the real data, each reconstruction was obtained segmented into connected components and was compared to the defect diagram. The results of applying this method to a variety of simulated and real data sets were then demonstrated, highlighting the strength of the proposed algorithm. Test structures similar to defects of interest were generated and simulated signals were also generated using the k-wave software [13] with a sensor geometry similar to the MIRA system. The result was then reconstructed using the normal SAFT algorithm and a related, MBIR-like technique based on a simple l_1 regularizer (referred to as *MBIR-*l_1). Figure 8 shows a qualitative comparison between MBIR and SAFT reconstruction from the k-wave simulated data. The far-left column shows the ground truth position of the defects. The next column to the right shows the SAFT reconstruction followed to the right by the two MBIR techniques with different regularizers. The MBIR-MRF results have significantly less noise and artifacts compared to the SAFT technique. Furthermore, the MBIR technique results in a significant improvement in eliminating noise, reconstruction artifacts, and resolving the shallow defects. This results in improved quantitative accuracy in detecting various defects, as evidenced in the PR curves in Figure 9.

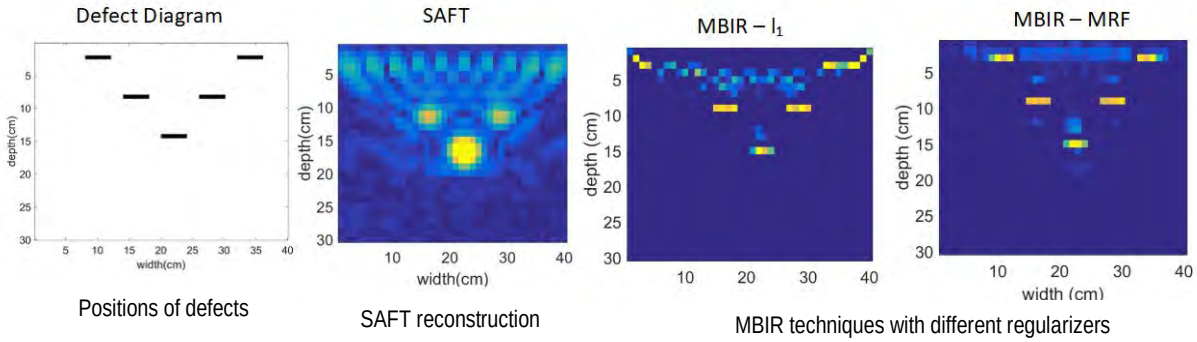

Figure 8. Qualitative comparison between MBIR and SAFT reconstruction from the k-wave simulated data; MBIR-MRF results have significantly less noise and artifacts compared to SAFT technique results.

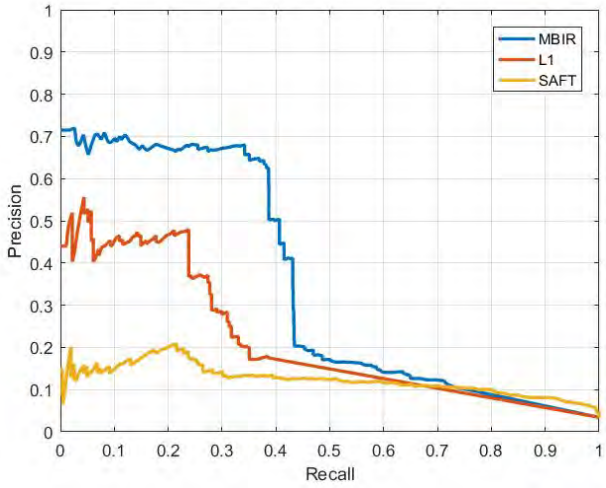

Figure 9. Quantitative comparison of algorithm performance based on PR curves for each technique over all simulation sets. Notice that MBIR outperforms SAFT by having the highest PR area.

The results were demonstrated by applying the method on real MIRA data sets obtained from a test concrete wall with known defects. The field of view of each cross section is 120 × 210 cm, and the reconstruction resolutions are 1 cm for all techniques. Figure 10 compares all reconstruction results from MIRA experimental data: the first column is the position of the defects, the second column is SAFT reconstruction, the third row is the l_1-norm reconstruction, and the fourth row is the MBIR reconstruction. MBIR tends to produce results with less noise and artifacts compared to other techniques. The MBIR technique shows significant enhancement in reducing artifacts and reducing noise compared with SAFT and l_1-norm techniques. The detection test (Figure 11) showed better quantitative performance of the ORNL MBIR-l_1 and MBIR-MRF algorithm over other techniques.

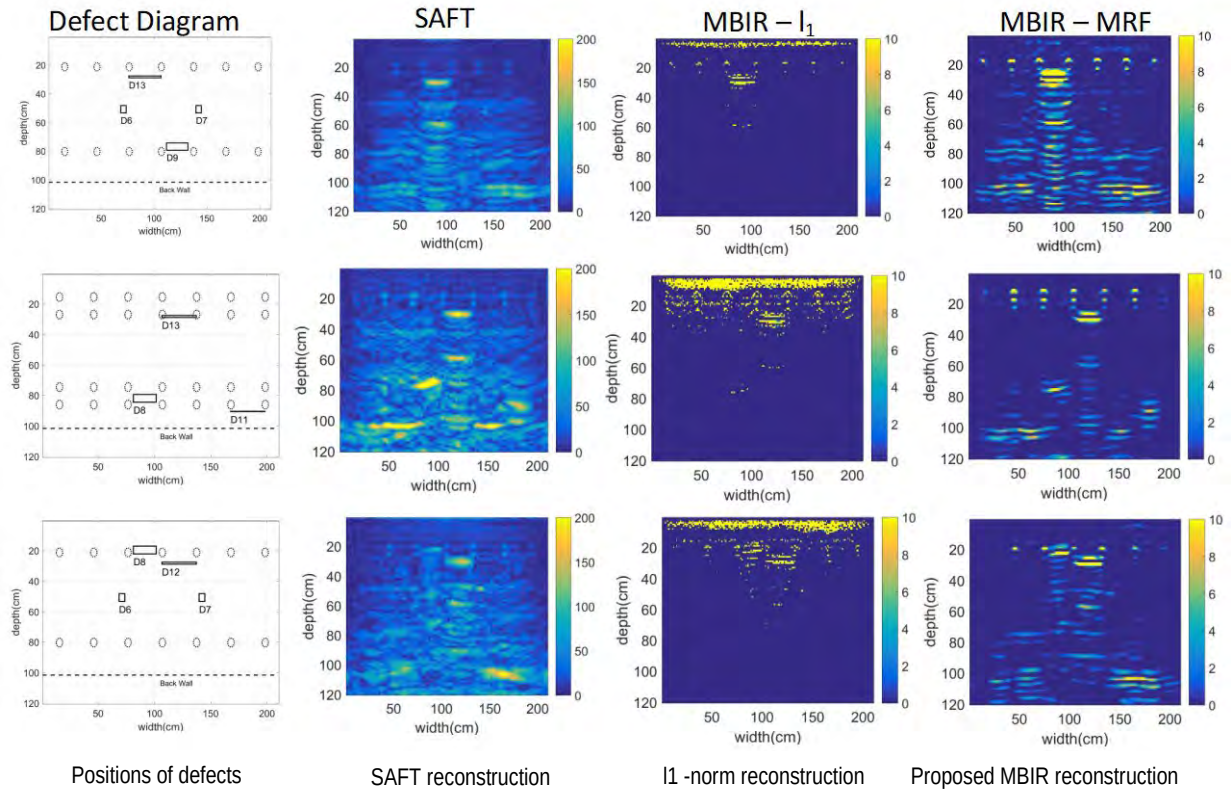

Figure 10. Comparison of all reconstruction results from the MIRA experimental data. MBIR reconstruction tends to produce results with less noise and artifacts compared to results obtained using other techniques.

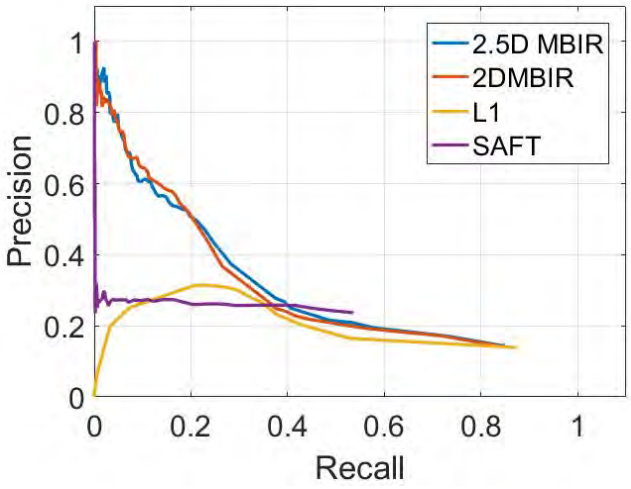

Figure 11. PR curves for each technique over all 73 slices in the MIRA experimental data. The proposed MBIR outperforms the other techniques.

5. DEVELOPMENT OF DIRECT-DEEP LEARNING FOR ULTRASOUND RECONSTRUCTIONS

The MBIR approach discussed above using a linear model resulted in significant improvements in reconstruction performance compared to SAFT while still being able to produce a reconstruction in near real-time. However, this linear-MBIR (L-MBIR) method still results in artifacts and cannot reconstruct objects buried deep in the sample because they are occluded by strong scattering due to the inherent non-linearity of the ultrasound forward model. Using a non-linear model in the MBIR approach is not feasible because the resulting optimization algorithm is computationally expensive and hence not suited for the near real-time reconstruction requirements of ultrasound NDE systems.

To address these challenges, an artificial intelligence (AI)–based algorithm was developed that can rapidly invert the ultrasound signals and obtain a high-quality reconstruction. This algorithm, termed *direct deep learning* (DDL) [12], works by training a deep convolutional neural network (CNN) to map the non-linear ultrasound measurements to the final 3D reconstruction. Specifically, examples of typical defects buried in concrete were generated and used to simulate the ultrasound measurements for the MIRA system using k-wave. Next, the CNN was trained to recover the original images from the non-linear simulated measurements. This CNN takes an image generated by applying a simple linear inversion algorithm such as SAFT to the simulated measurements and then maps it to the final reconstruction (see Figure 12). The inherent non-linearities in the CNN help account for the artifacts due to the non-linearities of ultrasound propagation.

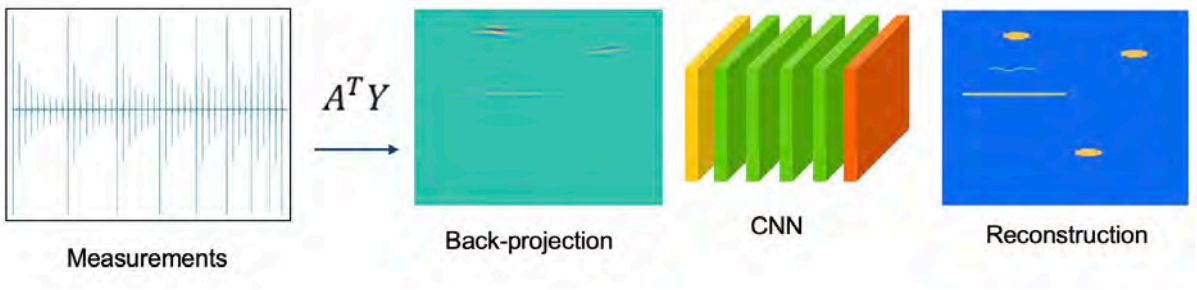

Figure 12. Overview of the DDL algorithm. The input measurements are first inverted using a simple linear mode, followed by a non-linear convolutional neural network. The network is trained using pairs of simulated measurements from synthetic images. For the CNN, a U-Net architecture is used with skip-connections (Figure 13) because such a network can account for multi-resolution features in the images.

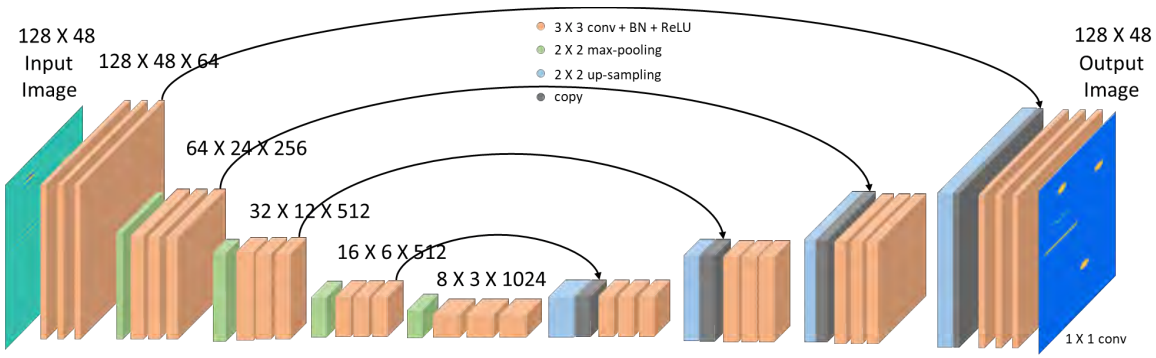

Figure 13. Modified U-net architecture used for the reconstructions. The input is an image obtained by applying the adjoint of a linear operator to the measurements. Within each stage, a 3 × 3 convolution is applied, followed by batch normalization and a rectified linear unit. The sizes of the feature maps at each stage are noted in the image.

To train the deep neural network, 1,800 images of size 48 × 32 pixels were used: 200 of the images were used for validation, and 200 were used for testing. The stochastic gradient descent (SGD) was used to optimize a loss function based on mean squared error between the prediction and the training data set. The optimization was stopped when the difference between the training and validation loss crossed a certain threshold.

Figure 14 shows a qualitative comparison of the reconstruction using SAFT, MBIR, and the proposed DDL algorithm. Notice that despite the non-linear propagation effects, it was possible to reconstruct the image accurately. The proposed DDL algorithm results in a dramatic improvement in image quality, reducing reverberation artifacts and being able to recover structures buried deep in the concrete. Figure 15 shows the precision-recall curves for the entire test data set of 200 images, illustrating how one could get a significant improvement of quantitative accuracy over the MBIR-l_1 and SAFT.

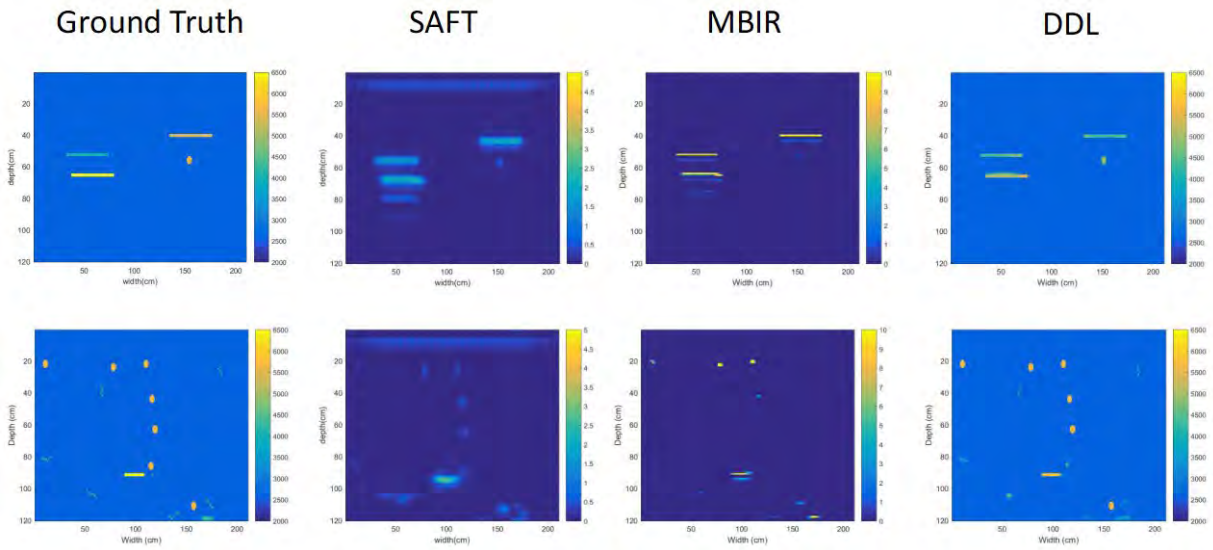

Figure 14. Comparison of all reconstruction results from k-wave simulation data from the test set only. DDL resulted in reconstructions with a dramatic reduction in artifacts and was able to image behind occluding objects, as seen in these cases.

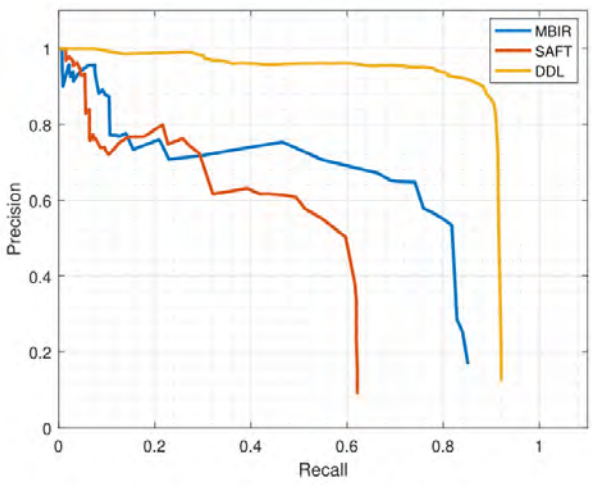

Figure 15. PR curves for each technique over all test data. The proposed DDL algorithm outperforms the other techniques.

Finally, ORNL is working on extending the DDL technique to real data sets by addressing the challenge of using a network trained purely on the simulated data compared to experimental data.

6. CONCLUSION

The nuclear industry is highly motivated to understand the material failures within plant infrastructures, and destructive testing is not a long-term option for investigating these structures. While NDE is a well-known, well-understood technology, the relationship between the measurement process and the material is less developed than the instrumentation. ORNL has developed several improved image reconstruction techniques, including frequency-banded SAFT (FB-SAFT) ultrasonic model-based iterative reconstruction (U-MBIR) and direct deep learning (DDL) reconstruction. These image reconstruction techniques aid in the ability to better understand the relationship between the measurements and the materials degradations.

This report reviews the progress of three reconstruction techniques under development at ORNL and discusses the improvement from SAFT to MBIR and DLL reconstructions. This technology could be integrated into fieldable instruments for improved real-time reconstructions (FB-SAFT) or higher quality image reconstructions with reduced noise and artifacts (MBIR or DDL).

7. REFERENCES

1. *Seabrook Station Safety in Light of Alkali-Silica Reaction Occurring in Plant Structures*. 2012; Available from: https://www.nrc.gov/reactors/operating/ops-experience/concrete-degradation.html.
2. *MIRA Tomographer spec sheet*. 2010 [cited 2019 August 2]; Available from: http://www.germann.org/TestSystems/MIRA%20Tomographer/MIRA%20Tomographer.pdf.
3. Clayton, D. A. and C. M. Smith. *Comparative testing of nondestructive examination techniques for concrete structures*. in *Nondestructive Characterization for Composite Materials, Aerospace*

Engineering, Civil Infrastructure, and Homeland Security 2014. 2014. International Society for Optics and Photonics.
4. Ezell, N. D. B., et al., *Comparison of Image Reconstruction Techniques Used for Nondestructive Evaluation of Thick-Concrete Specimens*. 2018, Oak Ridge National Lab.(ORNL), Oak Ridge, TN (United States).
5. Ezell, N. D. B., et al. *A novel use of frequency-banded synthetic aperture focusing technique for reconstructions of alkali-silica reaction in thick-reinforced concrete structures*. in *AIP Conference Proceedings*. 2019. AIP Publishing.
6. Hoegh, K. and L. Khazanovich, *Correlation analysis of 2D tomographic images for flaw detection in pavements.* 2011. **40**(2): p. 247-255.
7. Albright, A. and D. Clayton. *The benefits of using time-frequency analysis with synthetic aperture focusing technique*. in *AIP Conference Proceedings*. 2015. AIP.
8. Ezell, N. D. B., et al. *Detecting alkali-silica reaction in thick concrete structures using linear array ultrasound*. in *Nondestructive Characterization and Monitoring of Advanced Materials, Aerospace, Civil Infrastructure, and Transportation XII*. 2018. International Society for Optics and Photonics.
9. Clayton, D. A., et al., *Nondestructive evaluation of thick concrete using advanced signal processing techniques*. 2015, Oak Ridge National Lab.(ORNL), Oak Ridge, TN (United States).
10. Clayton, D. A., et al. *Automated Detection of Alkali-Silica Reaction in Concrete Using Linear Array Ultrasound Data*. in *Environmental Degradation of Materials in Nuclear Power Systems*. 2017. Springer.
11. Almansouri, H., et al., *Model-Based Iterative Reconstruction for One-Sided Ultrasonic Nondestructive Evaluation.* 2018. **5**(1): p. 150-164.
12. Almansouri, H., et al. *Deep neural networks for non-linear model-based ultrasound reconstruction*. in *2018 IEEE Global Conference on Signal and Information Processing (GlobalSIP)*. 2018. IEEE.
13. Treeby, B. E., M. Tumen, and B. T. Cox. *Time domain simulation of harmonic ultrasound images and beam patterns in 3D using the k-space pseudospectral method*. in *International Conference on Medical Image Computing and Computer-Assisted Intervention*. 2011. Springer.